ELSEVIER

Chemical Geology 225 (2006) 336–346

CHEMICAL GEOLOGY
INCLUDING
ISOTOPE GEOSCIENCE

www.elsevier.com/locate/chemgeo

Simulation of thermodynamic mixing properties of garnet solid solutions at high temperatures and pressures

Mikhail Yu. Lavrentiev [a,b,1], Wim van Westrenen [c,*], Neil L. Allan [a], Colin L. Freeman [a], John A. Purton [d]

[a] *School of Chemistry, University of Bristol, Cantock's Close, Bristol, BS8 1TS, UK*
[b] *Institute of Inorganic Chemistry, 630090 Novosibirsk, Russia*
[c] *Faculty of Earth and Life Sciences, Vrije Universiteit, De Boelelaan 1085, 1081 HV Amsterdam, The Netherlands*
[d] *CLRC, Daresbury Laboratory, Keckwick Lane, Warrington, WA4 4AD, UK*

Accepted 16 August 2005

Abstract

We present results of high temperature, high pressure atomistic simulations aimed at determining the thermodynamic mixing properties of key binary garnet solid solutions. Computations cover the pressure range 0–15 GPa and the temperature range 0–2000 K. Through a combination of Monte-Carlo and lattice-dynamics calculations, we derive thermodynamic mixing properties for garnets with compositions along the pyrope–almandine and pyrope–grossular joins, and compare these with existing experimental data. Across the pressure–temperature range considered, simulations show virtually ideal mixing behaviour in garnet on the pyrope–almandine join, while large excess volumes and enthalpies of mixing are predicted for garnet along the pyrope–grossular join. Excess heat capacities and entropies are also examined. These simulations shed additional light on the link between the behaviour at the atomic level and macroscopic thermodynamic properties: we illustrate the importance of certain atomistic Ca–Mg contacts in the pyrope–grossular solid solutions. For simulation techniques of this type to become sufficiently accurate for direct use in geological applications such as geothermobarometry, there is an urgent need for improved experimental determinations of several key quantities, such as the enthalpies of mixing along both joins.

Keywords: Solid solutions; Garnet; Computer simulation; Mixing properties; Monte-Carlo

1. Introduction

Aluminosilicate garnet [formula $X_3Al_2Si_3O_{12}$, with X a mixture of divalent Mg, Ca, Fe, and Mn cations] is one of the most important solid solutions in the Earth's crust and upper mantle. Garnet of varying composition is stable over a wide range of pressure–temperature conditions in a variety of metamorphic (e.g., amphibolites, eclogites) and igneous rocks (e.g., acid volcanics, peridotites). Because of their stability over a large part of pressure–temperature–bulk composition (*P–T–X*) space, garnet major element composition is commonly used in petrogenetic modelling (e.g., Nagel et al., 2002; Dale and Holland, 2003; Wei and Powell, 2003), with the aim of retrieving pressure/temperature conditions of

* Corresponding author. Tel.: +31 20 598 7279; fax: +31 20 646 2457.
E-mail address: wim.van.westrenen@falw.vu.nl (W. van Westrenen).
[1] Present address: EURATOM/UKAEA Fusion Association, Culham Science Centre, Oxfordshire, OX14 3DB, UK.

0009-2541/$ - see front matter © 2005 Elsevier B.V. All rights reserved.
doi:10.1016/j.chemgeo.2005.08.026

garnet growth or (re-)equilibration, and hence constraining part of a rock's *P–T* evolution.

As most minerals found in nature are solid solutions, thermodynamic databases used as input for modelling mineral compositions (e.g., Berman, 1988; Holland and Powell, 1998) require accurate parametrisations of thermodynamic mixing properties, i.e., volumes, enthalpies and entropies of mixing. In the case of garnet, this means activity–composition (*a–X*) relations for the major garnet end member components such as pyrope (Py), $Mg_3Al_2Si_3O_{12}$; grossular (Gr), $Ca_3Al_2Si_3O_{12}$; and almandine (Alm), $Fe_3Al_2Si_3O_{12}$ must be quantified. Several activity–composition relations for garnet solid solutions have been proposed (e.g., Berman, 1990; Berman and Aranovich, 1996; Ganguly et al., 1996; Mukhopadhyay et al., 1997; Holland and Powell, 1998). These models are partly based on phase equilibrium experiments, in which the garnet activity coefficients are measured by determining the *P–T* conditions of a phase boundary involving a range of garnet solid solutions in equilibrium with phases without solid solution (e.g., Berman, 1990; Koziol, 1990). Such experiments provide information on excess free energies of mixing. X-ray diffraction measurements of synthetic or natural garnet solid solutions (e.g., Merli et al., 1995; Geiger and Feenstra, 1997), providing information on excess volumes, have also been used. To disentangle the separate effects of excess enthalpy and entropy, calorimetric measurements on synthetic garnets (Newton et al., 1977; Geiger et al., 1987) have provided some constraints on enthalpies of mixing.

From these experimental studies, it is clear that some garnet solid solutions are highly non-ideal, especially those along the pyrope–grossular join, while other joins seem to exhibit near-ideal behaviour, e.g., pyrope–almandine. Unfortunately, agreement between the different models of garnet mixing properties based on experiments is not very satisfactory, prompting some authors to advise caution when using these models (e.g., Guiraud and Powell, 1996). In addition, little is known about the high pressure, high temperature evolution of garnet thermodynamic excess properties. In this study, we use alternative, computer-based methods to obtain thermodynamic excess properties as a function of pressure and temperature, through Monte-Carlo and lattice-dynamics simulations of garnet solid solutions at temperatures up to 2000 K and pressures up to 15 GPa. These conditions are well within the aluminosilicate garnet stability field for $X_3Al_2Si_3O_{12}$ systems. Pyrope–grossular garnets, for example, have been synthesised at 20 GPa and temperatures up to 2473 K (van Westrenen, unpublished data).

Non-ideal solid solutions present considerable challenges for simulation. Disorder in *solid* oxides has largely been investigated theoretically via point defect calculations (the dilute limit—for an overview see the special issue of J. Chem. Soc., Faraday Trans II, 1989), or via specific 'supercells' (e.g., Taylor et al., 1997), in which a superlattice of defects is introduced, extending throughout the macroscopic crystal. The periodicity is then that of the particular supercell chosen and convergence towards properties of an isolated defect occurs as the supercell size is increased. These methods are not readily extended to solid solutions.

We have developed a number of new codes to address such problems (Allan et al., 2001a; Lavrentiev et al., 2001). These are reviewed elsewhere in this special issue (Purton et al., 2005—this issue). A key feature is the requirement to sample many different arrangements of ions, allowing explicitly for the exchange of ions. Any method must also take into account the local environment of each ion and local structural movements (relaxation), which accompany any exchange of ions and in oxides and silicates reduce considerably the energy associated with any such interchange. Local effects due to ion association or clustering should not be averaged out. Methods should be readily extendible to incorporate the effects of high pressure or thermal (vibrational) effects. The use of parameterised Hamiltonians (e.g., of Ising type, see de Fontaine, 1994) is increasingly difficult beyond binary or pseudobinary alloys and so we have not used approximations of this type. The Monte-Carlo approach used here should be contrasted with the Cluster Variation Method (e.g., de Fontaine, 1994), recently applied to the pyrope–grossular solid solution at 1 bar by Vinograd et al. (2004) and Sluiter et al. (2004).

In this paper we extend earlier work (Lavrentiev et al., 2001; Todorov et al., 2004) on solutions of binary oxides (MnO–MgO and MgO–CaO) to the much more challenging problem of garnet solid solutions. We have chosen to study two representative garnet binaries, pyrope–grossular and pyrope–almandine. The pyrope–grossular system presents complications (as in our previous study of MgO–CaO) due to the large difference in ionic radius (Shannon, 1976) between Ca^{2+} (8-fold coordinated radius $r = 1.12$ Å) and Mg^{2+} (0.89 Å). In pyrope–almandine this mismatch is much smaller ($r(Fe^{2+}) = 0.92$ Å), so that together the two systems should provide a good test of our methods.

Fig. 1 shows the garnet structure, including the dodecahedral framework and the SiO_4 tetrahedra. A particularly striking feature of this mineral is the strong interaction between cations in dodecahedral sites linked via an

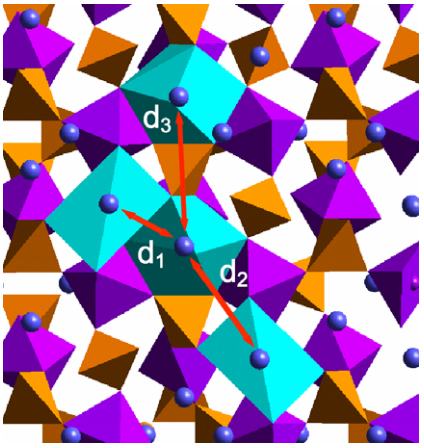

Fig. 1. Garnet structure showing SiO_4 tetrahedra (in yellow), AlO_6 octahedra (in purple), and the cations (dark blue) within their dodecahedra (light blue). The cation–cation 1st, 2nd and 3rd nearest neighbour distances are also shown as d_1, d_2 and d_3 respectively. (For interpretation of the references to colour in this figure legend, the reader is referred to the web version of this article.)

edge-shared tetrahedron, i.e., most unusually between *third* nearest cation neighbours (Bosenick et al., 2000; van Westrenen et al., 2003; Vinograd et al., 2004). Garnet solid solutions thus present a particularly interesting challenge for our new Monte-Carlo techniques.

2. Methods

We have used several computational techniques in this paper—static energy and direct free energy minimizations, Monte-Carlo (MC) simulations and configurational lattice-dynamics. These are reviewed in detail elsewhere in this issue (Purton et al., 2005—this issue). All calculations in this paper are based on an ionic model using the same set of two-body potentials and a three-body O–Si–O bond bending term to represent short-range forces, as implemented in our previous studies of garnets and garnet–melt trace element partitioning (van Westrenen et al., 2000, 2003). Two-body interatomic potentials are of the form $\varphi(r)=A\exp(-r/\rho)-C/r^6$, with r the interatomic distance, and a cut-off distance of 12 Å. The O–Si–O three-body bond bending term is given by $\varphi(\theta)=K_B(\theta-\theta_0)^2/2$, where θ is the O–Si–O angle. Account of the oxide ion polarisability was taken in all but the Monte-Carlo simulations by adding shells to the oxygen atoms following the model of Dick and Overhauser (1958).

2.1. Static energy minimisation

In the static limit (i.e., 0 K in the absence of lattice vibrations), the crystal structure is determined by the condition $\partial E/\partial X_i=0$, where E is the static contribution to the internal energy, and the variables $\{X_i\}$ define the structure (i.e., the lattice vectors, the atomic positions in the garnet unit cell, and the oxygen shell positions) (for more details see Catlow and Mackrodt, 1982). A detailed comparison of calculated static-limit and experimental structures of the end member garnets, almandine, pyrope and grossular and bulk moduli using the shell model potentials was included in our earlier work (van Westrenen et al., 2000, 2003) and is reproduced in Appendix A. A wide range of key crystal structural features were reproduced well, even if in some cases the difference between the end members is a little larger than that predicted. Our calculations are in the static limit at zero pressure, whereas experiment relates to room temperature and high pressure (3 GPa), so exact agreement should not be expected. In this paper, for all the calculations which incorporated shells (static and free energy minimizations, and configurational lattice-dynamics) we use the same well-tested interionic potentials and shell model parameters as in these earlier studies.

We have carried out an additional set of calculations on the end members at high pressure in the static limit using the SHELL code (Taylor et al., 1998) to compare with the experimental results of Zhang et al. (1998, 1999). For grossular over the pressure range 0–10.75 GPa the calculated lattice parameter a decreases by $\approx 1.7\%$, which compares with an experimental change of $\approx 1.8\%$ (Zhang et al., 1999). For pyrope over the pressure range 0–15.28 GPa, where basis atom positions are also available as a function of pressure (Zhang et al., 1998), calculated values of a, Ca–O(1), Ca–O(2), Al–O and Si–O decrease by $\approx 2.1\%$, 1.5%, 4.2%, 1.6% and 0.8% which corresponds to experimentally observed decreases of $\approx 2.5\%$, 2.0%, 4.9%, 1.8% and 1.0% respectively. For almandine over the pressure range 0–14.03 GPa the calculated lattice parameter a decreases by $\approx 2.0\%$, which compares with an experimental change of $\approx 2.2\%$ (Zhang et al., 1999). The agreement is very satisfactory.

2.2. Monte-Carlo

The majority of simulations in this paper are Monte-Carlo calculations, using a simulation cell size of 1280 ions containing 64 garnet formula units, and 5×10^6 steps, following initial equilibration of 2×10^6 steps (5×10^7 and 1×10^7 steps, respectively for pure end members). We use the same set of potentials as with the other methods (van Westrenen et al., 2000) but, as is standard practice with MC methods, within the frame-

work of a rigid ion model, i.e., without the addition of oxygen shells. Appendix A contains a more detailed comparison of properties calculated in the static limit using the shell and rigid models. We have checked convergence of the results with simulation cell size and number of simulation steps.

In this paper we make most use of Monte-Carlo Exchange (MCX) simulations (Purton et al., 1998), as for MnO–MgO (Allan et al., 2001b) and CaO–MgO (Lavrentiev et al., 2001). Here, at any step, as in the MC simulations, a random choice is made whether to attempt a random displacement of an ion, or a random change in the volume of the simulation box, and in addition whether to attempt a random exchange between two randomly selected atoms (see Purton et al., 2005—this issue for more details). The Metropolis algorithm is used to accept or reject any attempted move (Eppinga and Frenkel, 1984). For both pyrope–grossular and pyrope–almandine solid solutions, as for CaO–MgO and $MgAl_2O_4$ (spinel) previously, we have applied the biased sampling technique to speed up the sampling of configurations. For each accepted configuration the desired thermodynamic and structural properties are calculated and, at the end of the calculation, the average values of these quantities are obtained.

2.3. Free energy minimisation

An alternative method for the calculation of thermodynamic properties of a *periodic* solid at finite temperature and high pressure is via the direct minimisation of the free energy (rather than just the static energy) with respect to the variables $\{X_i\}$ which define the structure. We use quasiharmonic lattice-dynamics (QLD) for the vibrational terms, as implemented in the program SHELL (Taylor et al., 1998).

Our *configurational lattice-dynamics* (CLD) method (Allan et al., 2001a; Todorov et al., 2004) for *mineral solid solutions* builds on this full free energy minimisation of periodic solids, since the calculation of the free energy to high precision using QLD is quick and computationally efficient (Taylor et al., 1998). CLD involves the evaluation of an appropriate thermodynamic average over a (limited) set of calculations representing different arrangements of the cations within a supercell.

In principle CLD involves the full free energy minimization of each configuration at each P and T of interest. Optimisation of each configuration in the static limit is computationally much cheaper. When reference is made later to thermodynamic properties of the solid solutions in the static limit, configurationally averaged values are evaluated replacing the free energy of each configuration k with the static energy E_k. The temperature enters only through the thermodynamic (Boltzmann) averaging. The vibrational contribution to E_k and the vibrational entropy are ignored. The minimization of each configuration is computationally much cheaper and for *all* temperatures only *one* set of runs for a given composition is required. See Todorov et al. (2004) and Purton et al. (2005—this issue) for a detailed discussion.

3. Results and discussion

3.1. Enthalpies of mixing

For Py–Gr solid solutions we plot in Fig. 2 enthalpies of mixing ($\Delta_{mix}H$) at 1500 K and five pressures up to 15 GPa, calculated using Monte-Carlo (MCX) simulations. These are all positive with a dip at lower pressures at a composition of ≈ 50:50, possibly hinting at some preferential ordering. The statistical errors (standard deviation) for these enthalpies are ≈ 0.004%. Available experimental data (Newton et al., 1977) at atmospheric pressure are also shown. These, like the calculated values, are positive and show similar asymmetry, with higher values for pyrope-rich garnet. Quantitative agreement is, however, rather poor. For example the calculated enthalpy of mixing for composition $Py_{50}Gr_{50}$ is 14.75 kJ per mole of formula unit, while the experimental value (at composition $Py_{53}Gr_{47}$) is ≈ 8.2 kJ/mol.

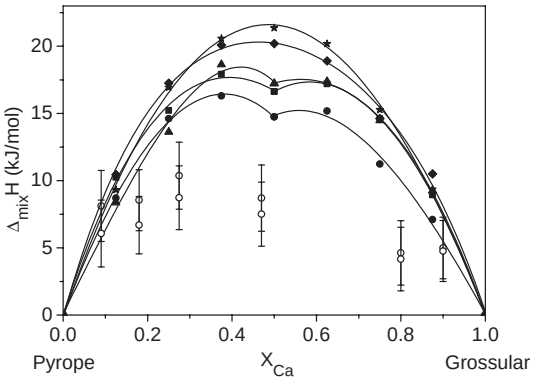

Fig. 2. Calculated enthalpy of mixing along the pyrope–grossular join at temperature T=1500 K, atmospheric pressure (closed circles), pressure P=3 GPa (triangles), P=5 GPa (squares), P=10 GPa (diamonds), P=15 GPa (stars). Experimental data from Newton et al. (1977) (open circles) shown for comparison. Two open circles at each composition derived by assuming minimum and maximum values for the enthalpy of end member pyrope measured by Newton et al. (1977).

We return to this below in the context of the temperature dependence of $\Delta_{mix}H$.

Fig. 3 plots the analogous calculated enthalpies of mixing at atmospheric pressure and 1500 K for pyrope–almandine. These values are all positive but much smaller than those for Py–Gr, as might be expected given the smaller size mismatch between Mg^{2+} and Fe^{2+} compared with that between Mg^{2+} and Ca^{2+}. The calculated values are also consistent with the scaling arguments of Bosenick et al. (2001). Comparison with the experimental results of Geiger et al. (1987), also shown in Fig. 3, shows that agreement is reasonable at high Py concentrations but that a significant discrepancy exists at almandine-rich compositions, where the experimental values are more positive and increase with increasing almandine content. In this context it is worth noting the unavoidable, but largely unknown effect of the presence of octahedrally coordinated trivalent iron on the measured enthalpy of almandine-rich garnet (e.g., Geiger and Feenstra, 1997).

At atmospheric pressure, the calculated enthalpy of mixing for $Py_{50}Gr_{50}$ decreases with decreasing temperature (by ≈ 2 kJ mol^{-1} from 1600 K to 1000 K). The magnitude of the change is such that agreement between simulation and the data of Newton et al. (1977), obtained at a temperature of 970 K, remains poor. Similarly the enthalpy of mixing results of the static limit calculations of Bosenick et al. (2000, 2001) are larger than these experimental data by a factor of ≈ 1.5.

We have also estimated $\Delta_{mix}H$ for $Py_{50}Gr_{50}$ at atmospheric pressure and 1500 K using CLD calculations and generating energies of individual configurations in the static limit. A cubic cell of 160 atoms and $\approx 27{,}610$ configurations is used for all the CLD simulations reported. These indicate a value of ≈ 20 kJ mol^{-1}, compared to a value of ≈ 21 kJ mol^{-1} for the MCX simulations at similar P–T conditions. This is likely to be an overestimate due to the relatively small cell size used here and also the use of the static limit, ignoring vibrational contributions (see Todorov et al., 2004). Nevertheless, this value of $\Delta_{mix}H$ is greater than the Monte-Carlo value for the same composition and thus the discrepancy with the experimental value remains.

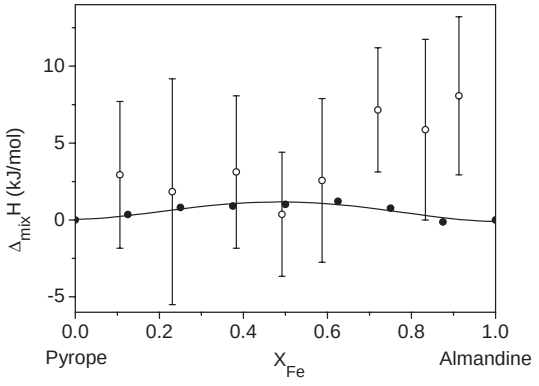

Fig. 3. Calculated enthalpy of mixing along the pyrope–almandine join at $T=1500$ K and atmospheric pressure (closed circles). Experimental data from Geiger et al. (1987) (open circles) shown for comparison.

One possible explanation for the disagreement between simulation and experiment is the particular interionic potential model we have used. However the available calorimetric measurements are themselves subject to large uncertainties. For example, Newton et al. (1977) provide three measurements of the enthalpy of pure end member pyrope that differ by up to 3.2 kJ mol^{-1}; the data plotted in Fig. 2 are the maximum and minimum $\Delta_{mix}H$ obtained depending on which of these three values are used. A comparison of the experimental data in Figs. 2 and 3 suggests that for some Mg-poor compositions the experimentally determined enthalpy of mixing of Py–Alm is higher than that of Py–Gr, which is unlikely given the size differences of the X-site cations involved. Given all these factors and the previous successes of our potential model, we have chosen not to alter the set of potentials. Concurring with Geiger (1999), our results here and those of Bosenick et al. (2000, 2001), Vinograd et al. (2004) and Sluiter et al. (2004), all of whom use different potentials, suggest that an experimental re-examination of the enthalpy of mixing of both the Py–Gr and Py–Alm binaries is highly desirable.

3.2. Volumes of mixing

In Fig. 4, calculated Monte-Carlo excess volumes ($\Delta_{mix}V$) for pyrope–grossular are compared with experimental data. Statistical errors (standard deviations) are typically $\approx 0.02\%$. The volume of mixing along the pyrope–grossular join is large and positive, as observed experimentally (Ganguly et al., 1993; Bosenick and Geiger, 1997). Most recent studies do not support negative volumes of mixing in any aluminosilicate binaries.

Our results are in better quantitative agreement with experiment than for the enthalpies of mixing, although in general our values are on the high side and possibly less asymmetric. It is important to bear in mind that again experimental uncertainties are relatively large. Our CLD calculations in the static limit, as described above, suggest an estimate of ≈ 0.48 cm^3 mol^{-1} for the

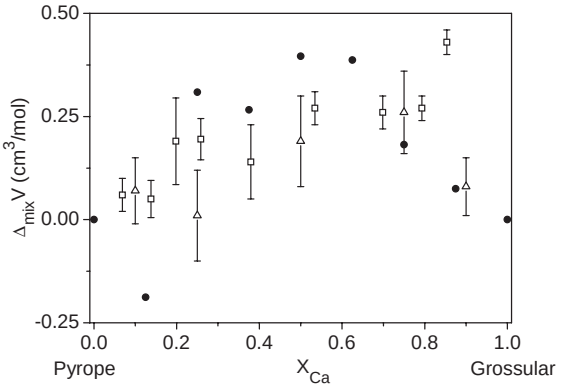

Fig. 4. Calculated volume of mixing along the pyrope–grossular join at $T=1500$ K and atmospheric pressure (circles). Experimental values ($T=295$ K, $P=1$ bar) from Ganguly et al. (1993) (squares) and Bosenick and Geiger (1997) (triangles) shown for comparison.

$Py_{50}Gr_{50}$ solid solution, in reasonable agreement with experiment and the MC results. Our values are also close to those of Sluiter et al. (2004) obtained from a small number of ab initio calculations. The calculated values of Vinograd et al. (2004) are a factor of four less than our own.

In contrast, volumes of mixing along the pyrope–almandine join are small (between 0 and 0.05 cm^3 mol^{-1}). This agrees with the measurements of Geiger and Feenstra (1997) (see also Geiger, 2000) who conclude the experimental data are indistinguishable from ideal behaviour.

Fig. 5 shows the variation of the volume of mixing as a function of pressure for $Py_{50}Gr_{50}$ at 1500 K, for which there are no experimental data for comparison. This figure shows $\Delta_{mix}V$ decreases with increasing pressure for this composition, as it does also for all other compositions along this join.

3.3. Other thermodynamic properties of mixing

The heat capacity of mixing of $Py_{60}Gr_{40}$ has been measured at low temperatures by Haselton and Westrum (1980). The results show a strong positive excess with a maximum at ≈ 50 K. We have calculated the heat capacity of mixing for $Py_{50}Gr_{50}$ at atmospheric pressure as a function of temperature using the free energy minimisation technique described by Purton et al. (2005—this issue) and a uniform grid of 8000 wavevectors in the Brillouin zone. We have used only the lowest energy configuration for a unit cell of 160 atoms in which there are no Ca–Ca or Mg–Mg third neighbour interactions, as discussed by van Westrenen et al. (2003) and to which we refer further below.

Fig. 6(a) compares calculated results ($Py_{50}Gr_{50}$) with the experimental data. The position of the positive maximum at ≈ 50 K is well reproduced by the simulation, and both simulation and experiment indicate a small region of negative excess at somewhat higher temperatures. Experiment and simulation appear not to be in such good agreement as to the magnitude of the 50 K peak, but it is important to stress our calculations are for a different cation composition than that used experimentally ($Py_{60}Gr_{40}$) and we have used only one configuration in the calculation.

Fig. 6(b) and (c) compare the calculated vibrational (phonon) densities of states of the $Py_{50}Gr_{50}$ solid solution at 300 K with the densities of the two end-members at the same temperature; the latter are in good agreement with those calculated by Mittal et al. (2001). There is a marked increase in frequencies at the lowest wavenumbers compared with that expected from the average of the end members. This is in line with previous suggestions (Haselton and Westrum, 1980; Geiger et al., 1992; Geiger, 2001) that the positive heat capacity of mixing is associated with the slightly larger Mg–O dodecahedra in the solid solution compared with those in pyrope itself.

It is also of interest to consider the excess vibrational entropies. For $Py_{50}Gr_{50}$ and again using only the lowest energy configuration, we obtain an estimate of ≈ 3.5 J K^{-1} mol^{-1} at 300 K. This value is approximately three times the estimated values of Vinograd et al. (2004).

Estimating the configurational entropy of mixing for the 50:50 composition as described by Todorov et al. (2004), using the same 27,610 configurations as previously for the enthalpy of mixing gives values -1.7 J K^{-1} mol^{-1} at 1500 K and ≈ -5.9 J K^{-1} mol^{-1} at 300 K less than the ideal value. The reduction in the configurational entropy from the ideal value, due to clus-

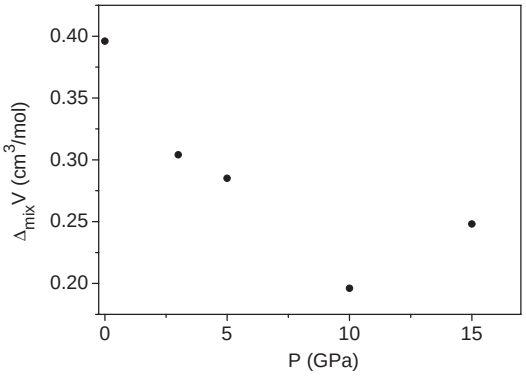

Fig. 5. Calculated volume of mixing of $Py_{50}Gr_{50}$ as a function of pressure at constant temperature $T=1500$ K.

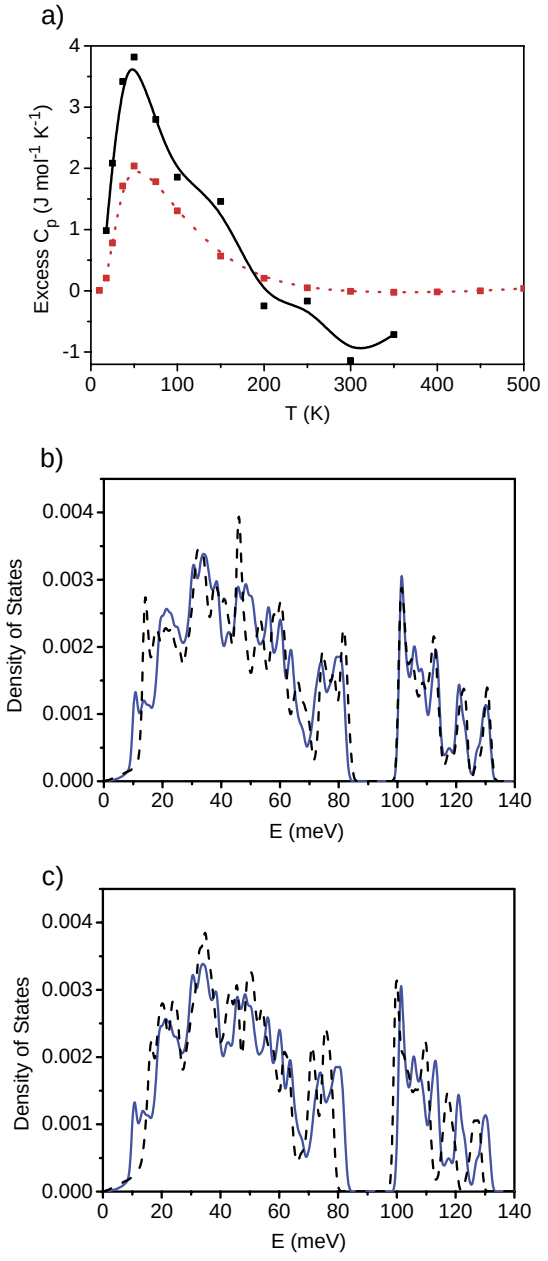

Fig. 6. (a) Comparison between excess heat capacity at atmospheric pressure calculated using QLD for $Py_{50}Gr_{50}$ (dotted line) and experimental results for $Py_{60}Gr_{40}$ (Haselton and Westrum, 1980) (solid line). (b,c) Calculated phonon densities of states (DOS) at atmospheric pressure for $Py_{50}Gr_{50}$ (solid line) compared with calculated DOS for (b) end member pyrope (dashed line), (c) end member grossular (dashed line).

tering of Mg and Ca ions, compared to a completely random distribution, is small at the higher temperature in good agreement with the simulations of Bosenick et al. (2000) and we return to consider this further in a later section. For comparison Geiger (2001) suggests values of ≈ -1 J K^{-1} mol^{-1} at 1273 K and ≈ -5 J K^{-1} mol^{-1} at 500 K.

3.4. Bulk moduli and thermal expansivity

At ambient temperature and pressure, experimental values of the end member bulk moduli K_T are 171–179 GPa (pyrope), 166–174 GPa (grossular) and 168–178 GPa (almandine) respectively (e.g., Conrad et al., 1999). In the static limit (0 K but in the absence of lattice vibrations) the calculated moduli are 214 GPa (pyrope), 194 GPa (grossular) and 208 GPa (almandine). At 1500 K values determined from our Monte-Carlo simulations are 175 GPa (pyrope), 164 (grossular) and 172 (almandine). Typical Monte-Carlo errors (standard deviations) are $\approx 4\%$ for the bulk modulus. Thus although the calculated values are in excess of those determined experimentally, the temperature variation of K_T is reasonable given that garnet bulk moduli typically decrease by 7 GPa for an increase in temperature of 300 K (e.g., Anderson and Isaak, 1995).

We have also calculated the thermal expansion of pyrope and grossular using two simulation techniques (Fig. 7). Over the temperature range 0–1000 K we have used direct full free energy minimisation at each temperature (full circles) and above 1000 K, where the quasi-harmonic approximation fails, Monte-Carlo (black triangles). Typical Monte-Carlo uncertainties (standard deviations) are $\approx 14\%$ for the expansion coefficient. The resulting variation of the volumetric thermal expansion α is shown in Fig. 7 together with available experimental data (as analysed by Bosenick and Geiger, 1997). Agreement is very good and shows the expansivities of pyrope and grossular are very similar.

Recently Walker et al. (2002) have called attention to the variation of quantities such as the bulk modulus and the thermal expansion coefficient across the join in binary mixtures of alkali halides. In line with their experimental results for NaCl–KCl we find a non-linear variation of K_T with composition along the pyrope–grossular join, with, for example, bulk moduli for the intermediate garnets 4–6 GPa lower at 1500 K and atmospheric pressure than expected from a linear interpolation between the end members. Unfortunately the similarity of the thermal expansion coefficients of pyrope and grossular at high temperatures together with the large uncertainties in the results for this quantity obtained from the numerical differentiation of the Monte-Carlo volumes mean that it is not possible to draw conclusions regarding the behaviour of the thermal expansion across the join at this stage.

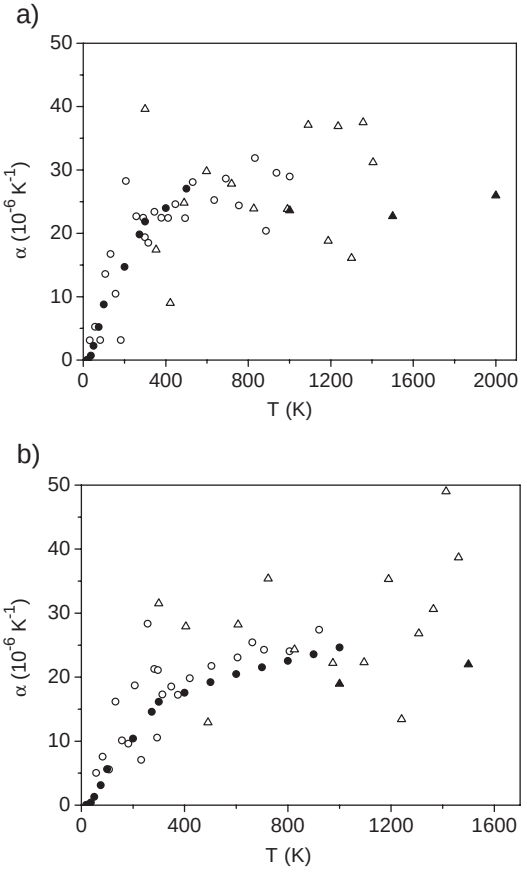

Fig. 7. Thermal expansivity of (a) pyrope and (b) grossular as a function of temperature at atmospheric pressure. Calculations: QLD (solid circles), MC (solid triangles). Experimental data from Bosenick and Geiger (1997, open circles) and Thiéblot et al. (1998, open triangles) shown for comparison.

3.5. Third neighbour interactions

So far we have considered a range of thermodynamic properties of garnet solid solutions, highlighting areas where new experiments would be very worthwhile. We now turn to consider how the atomic scale behaviour of the garnet solid solution influences these thermodynamic properties and in particular non-ideality.

Limited short-range Ca–Mg ordering in intermediate Py–Gr garnet has been suggested previously, e.g., the ^{29}Si MAS NMR studies of Bosenick et al. (1995, 1999). Possible orderings have also been examined computationally (Bosenick et al., 2000; van Westrenen et al., 2003). A particularly interesting conclusion of these studies and that of Vinograd et al. (2004) is that by far the strongest cation–cation interaction is that between dodecahedral sites linked via an edge-shared tetrahedron, i.e., between *third* nearest cation neighbours, as shown in Fig. 1. Accordingly we have monitored the nature of the third neighbour interactions in $Py_{50}Gy_{50}$ and $Py_{50}Alm_{50}$ from Monte-Carlo simulations as a function of temperature. Note that for technical reasons these calculations were carried out on the primitive cubic unit cell (160 atoms) which predicts slightly larger ($\approx 15\%$) values of $\Delta_{mix}H$ than the values converged with respect to cell size presented earlier. Fig. 8 plots the number of third nearest neighbour Mg–Mg pairs as a fraction of the total of third neighbour pairs. An entirely random arrangement of cations would give rise to a value of 0.25 for this quantity. It is clear from this figure that pyrope–almadine is behaving essentially as an ideal solution, with a random distribution of third neighbours, and this is fully consistent with the calculated thermodynamic properties presented earlier.

The pyrope–grossular solid solution is very different in that at low temperatures there are very few Mg–Mg third neighbour pairs. In line with the work of Bosenick et al. (2000), configurations containing Mg–Mg and Ca–Ca third-neighbour interactions are nevertheless energetically accessible at elevated temperatures. Bosenick et al. (1999) have shown that the extent of local Ca–Mg ordering observed experimentally is a function of garnet synthesis temperature, consistent with the trend shown in Fig. 8. We have discussed previously (van Westrenen et al., 2003) the major implications of this ordering for trace-element garnet–melt partitioning.

At higher pressures the number of Mg–Mg third nearest neighbour pairs increases in the pyrope–grossular solution, as also shown in Fig. 8. This is consistent with the different compressibilities of the Mg and Ca dodecahedral sites, with the Ca site more easily

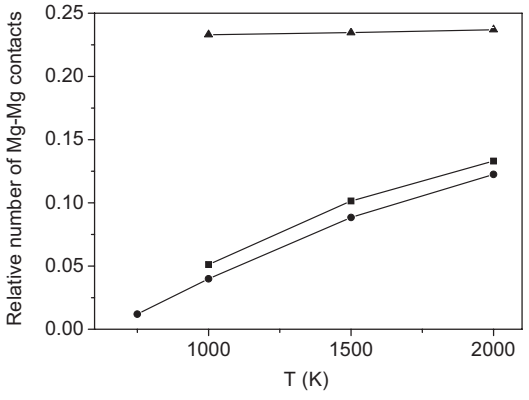

Fig. 8. Relative number of Mg–Mg contacts as a function of temperature for $Py_{50}Gr_{50}$ (circles, atmospheric pressure; squares, pressure $P=1.5$ GPa) and $Py_{50}Al_{50}$ (triangles, atmospheric pressure) taken from calculations. The relative number of contacts expected for a random distribution of garnet X-site cations is 0.25.

compressible and thus making the Mg and Ca sites less different at higher pressures. This is also associated with the disappearance of the small dip in the composition variation of the enthalpies of mixing at higher pressures (Fig. 2) and the decrease in $\Delta_{mix}H$ with increasing pressure.

4. Conclusions

In this paper we have extended previous simulation studies of garnet in the static limit to consider a wide range of calculated thermodynamic properties of garnet solid solutions at elevated temperatures and pressures, and linked these where possible to ordering on the atomic scale. Overall, the pyrope–almadine solution is calculated to be near ideal, while the simulated pyrope–grossular solution, involving a larger cation size mismatch, is strongly non-ideal over the complete P–T range studied. Our results indicate an urgent need for new experimental determinations of several key quantities, such as the enthalpies of mixing along both joins. Such measurements are critical not only to be able to refine models and methods, but are essential if simulations of this type are to become sufficiently accurate to be able to be used in quantitative applications such as geothermobarometry.

Acknowledgements

We wish to thank Charles Geiger for organizing the EMU workshop on 'Solid Solutions in Silicate and Oxide Systems' which prompted this work. MYL and CLF thank EPSRC for funding. Computational resources were made available thanks to a number of JREI awards to NLA. This paper benefited from discussions with Fraukje Brouwer and Roger Powell on garnet thermodynamics, and from comments by Udo Becker and two anonymous reviewers. **[LMW]**

Appendix A

In this appendix we present a table comparing experimental and calculated end member structures. All calculations are in the static limit; the shell model set (van Westrenen et al., 2000) uses the same set of interionic potentials as the rigid ion set but with the addition of shells on oxygen. van Westrenen et al. (2003) present the same comparisons as here, but only for the shell model set.

Property (unit)	Pyrope			Grossular			Almandine		
	Observed[a]	Simulated		Observed[b]	Simulated		Observed[a]	Simulated	
		Shell model	Rigid-ion model		Shell model	Rigid-ion model		Shell model	Rigid-ion model
Unit cell dimensions and oxygen atom co-ordinates									
a (Å)	11.452	11.281	11.392	11.848	11.874	11.937	11.525	11.386	11.490
b (Å)	11.452	11.281	11.392	11.848	11.874	11.937	11.525	11.386	11.490
c (Å)	11.452	11.281	11.392	11.848	11.874	11.937	11.525	11.386	11.490
x(O)	0.0329	0.0318	0.0371	0.0382	0.0385	0.0417	0.0340	0.0329	0.0378
y(O)	0.0503	0.0519	0.0421	0.0453	0.0458	0.0339	0.0494	0.0497	0.0403
z(O)	0.6533	0.6519	0.6545	0.6514	0.6493	0.6530	0.6527	0.6514	0.6542
Dodecahedron (X-site)									
X–O (1) (Å)	2.197	2.168	2.197	2.322	2.331	2.338	2.221	2.194	2.219
X–O (2) (Å)	2.340	2.283	2.430	2.487	2.542	2.648	2.371	2.331	2.472
<X–O> (Å)	2.269	2.225	2.313	2.405	2.437	2.493	2.296	2.263	2.346
O4–O6 (Å)	2.708	2.649	2.853	2.971	3.076	3.195	2.764	2.725	2.916
O4–O7 (Å)	2.778	2.721	2.833	2.859	2.923	3.019	2.796	2.761	2.874
Octahedron (Y-site)									
Al–O (Å)	1.886	1.846	1.873	1.926	1.894	1.936	1.890	1.853	1.882
O1–O4 shared (Å)	2.617	2.541	2.687	2.758	2.747	2.870	2.642	2.575	2.718
O1–O5 unshared (Å)	2.716	2.678	2.609	2.689	2.613	2.599	2.704	2.665	2.605
Tetrahedron (Z-site)									
Si–O (Å)	1.634	1.635	1.554	1.646	1.649	1.579	1.635	1.637	1.559
O1–O2 (Å)	2.497	2.505	2.378	2.572	2.580	2.453	2.509	2.515	2.387
O1–O3 (Å)	2.751	2.749	2.615	2.745	2.743	2.639	2.747	2.749	2.621

[a] Pyrope and almandine data from Armbruster et al. (1992).
[b] Grossular data from Ganguly et al. (1993).

References

Allan, N.L., Blundy, J.D., Purton, J.A., Lavrentiev, M.Yu., Wood, B.J., 2005—this issue. Trace element incorporation in minerals and melts. In: Geiger, C.A., Papp, G., Weiszburg, T.G. (Eds.), Solid Solutions in Silicate and Oxide Systems. Volume 3 of European Mineralogical Union Notes in Mineralogy. Eötvös University Press, pp. 251–302.

Allan, N.L., Barrera, G.D., Lavrentiev, M.Yu., Todorov, I.T., Purton, J.A., 2001b. Ab initio calculation of phase diagrams of ceramics and minerals. J. Mater. Chem. 11, 63–68.

Anderson, O.L., Isaak, D.G., 1995. Elastic constants of mantle minerals at high temperature. In: Ahrens, T.J. (Ed.), Mineral physics and crystallography—a handbook of physical constants. AGU Reference Shelf, vol. 2. American Geophysical Union, pp. 64–97.

Armbruster, T., Geiger, C.A., Lager, G.A., 1992. Single-crystal X-ray structure of synthetic pyrope almandine garnets at 100 and 293 K. Am. Mineral. 77, 512–521.

Berman, R.G., 1988. Internally-consistent thermodynamic data for minerals in the system Na_2O–K_2O–CaO–MgO–FeO–Fe_2O_3–Al_2O_3–SiO_2–TiO_2–H_2O–CO_2. J. Petrol. 29, 445–522.

Berman, R.G., 1990. Mixing properties of Ca–Mg–Fe–Mn garnets. Am. Mineral. 75, 328–344.

Berman, R.G., Aranovich, L.Y., 1996. Optimized standard state and solution properties of minerals: I. Model calibration for olivine, orthopyroxene, cordierite, garnet, and ilmenite in the system FeO–MgO–CaO–Al_2O_3–TiO_2–SiO_2. Contrib. Mineral. Petrol. 126, 1–24.

Bosenick, A., Geiger, C.A., 1997. Powder X-ray diffraction study of synthetic pyrope–grossular garnets between 20 and 295 K: a comparison of thermal expansion and heat capacity and volumes of mixing. J. Geophys. Res. 102, 22, 649–22,657.

Bosenick, A., Geiger, C.A., Schaller, T., Sebald, A., 1995. A ^{29}Si MAS NMR and IR spectroscopic investigation of synthetic pyrope–grossular garnet solid-solutions. Am. Mineral. 80, 691–704.

Bosenick, A., Geiger, C.A., Phillips, B.L., 1999. Local Ca–Mg distribution of Mg-rich pyrope–grossular garnets synthesized at different temperatures revealed by ^{29}Si MAS NMR spectroscopy. Am. Mineral. 84, 1423–1433.

Bosenick, A., Dove, M.T., Geiger, C.A., 2000. Simulation studies on the pyrope–grossular solid solution. Phys. Chem. Miner. 27, 398–418.

Bosenick, A., Dove, M.T., Heine, V.A., Geiger, C.A., 2001. Scaling of thermodynamic mixing properties in garnet solid solutions. Phys. Chem. Miner. 28, 177–187.

Catlow, C.R.A., Mackrodt, W.C., 1982. Computer simulation of solids. In: Catlow, C.R.A., Mackrodt, W.C. (Eds.), Computer Simulations of Solids. Springer-Verlag, Berlin. Chapter 1.

Conrad, P.G., Zha, C.-S., Mao, H., Hemley, R.J., 1999. The high-pressure, single-crystal elasticity of pyrope, grossular and andradite. Am. Mineral. 84, 374–383.

Dale, J., Holland, T.J.B., 2003. Geothermobarometry, *P*–*T* paths and metamorphic field gradients of high-pressure rocks from the Adula Nappe, Central Alps. J. Metamorph. Geol. 21, 813–829.

de Fontaine, D., 1994. Cluster approach to order–disorder transformations in alloys. Solid State Phys. 47, 33–176.

Dick, B.G., Overhauser, A.W., 1958. Theory of the dielectric constants of alkali halide crystals. Phys. Rev. 112, 90–103.

Eppinga, P., Frenkel, D., 1984. Monte Carlo study of the isotropic and nematic phases of infinitely thin hard platelets. Mol. Phys. 52, 1303–1334.

Ganguly, J., Cheng, W., O'Neill, H.St.C., 1993. Syntheses, volume and structural changes of garnets in the pyrope–grossular join: implications for stability and mixing properties. Am. Mineral. 78, 583–593.

Ganguly, J., Cheng, W., Tirone, M., 1996. Thermodynamics of aluminosilicate garnet solid solutions: new experimental data, an optimized model, and thermometric applications. Contrib. Mineral. Petrol. 126, 137–151.

Geiger, C.A., 1999. Thermodynamics of $(Fe^{2+},Mn^{2+},Mg,Ca)_3Al_2Si_3O_{12}$ garnet: an analysis and review. Mineral. Petrol. 66, 271–299.

Geiger, C.A., 2000. Volumes of mixing in aluminosilicate garnets: implications for solid-solution behaviour. Am. Mineral. 85, 893–897.

Geiger, C.A., 2001. Thermodynamic mixing properties of binary oxide and silicate solid solutions determined by direct measurements: the role of strain. In: Geiger, C.A., Papp, G., Weiszburg, T.G. (Eds.), Solid solutions in silicate and oxide systems. Volume 3 of European Mineralogical Union Notes in Mineralogy. Eötvös University Press, pp. 71–100.

Geiger, C.A., Feenstra, A., 1997. Molar volumes of mixing of almandine–pyrope and almandine–spessartine garnets and the crystal chemistry and thermodynamic properties of the aluminosilicate garnets. Am. Mineral. 82, 571–581.

Geiger, C.A., Newton, R.C., Kleppa, O.J., 1987. Enthalpy of mixing of synthetic almandine–grossular and almandine–pyrope from high-temperature solution calorimetry. Geochim. Cosmochim. Acta 51, 1755–1763.

Geiger, C.A., Merwin, L., Sebald, A., 1992. Structural investigation of pyrope garnet using temperature dependent FTIR and ^{29}Si and ^{27}Al MAS NMR spectroscopy. Am. Mineral. 77, 713–717.

Guiraud, M., Powell, R., 1996. How well known are the thermodynamics of Fe–Mg–Ca garnet? Evidence from experimentally determined exchange equilibria. J. Metamorph. Geol. 14, 75–84.

Haselton, H.T., Westrum, E.F., 1980. Low-temperature heat capacities of synthetic pyrope, grossular and $pyrope_{60}grossular_{40}$. Geochim. Cosmochim. Acta 44, 701–709.

Holland, T.J.B., Powell, R., 1998. An internally-consistent thermodynamic data set for phases of petrological interest. J. Metamorph. Geol. 16, 309–343.

J. Chem. Soc., Faraday Trans II, 1989. Fifty Years of the Mott–Littleton approximation. J. Chem. Soc., Faraday Trans II 85, 335–579.

Koziol, A.M., 1990. Activity–composition relationships of binary Ca–Fe and Ca–Mn garnets determined by reversed, displaced equilibrium experiments. Am. Mineral. 75, 319–327.

Lavrentiev, M.Yu., Allan, N.L., Barrera, G.D., Purton, J.A., 2001. Ab initio calculation of phase diagrams of ceramics. J. Phys. Chem., B 105, 3594–3599.

Merli, M., Callegari, A., Cannillo, E., Caucia, F., Leona, M., Oberti, R., Ungaretti, L., 1995. Crystal–chemical complexity in natural garnets: structural constraints on chemical variability. Eur. J. Mineral. 7, 1239–1249.

Mittal, R., Chaplot, S.L., Choudbury, N., 2001. Lattice-dynamics calculations of the phonon spectra and thermodynamic properties of the aluminosilicate garnets pyrope, grossular, and spessartine $M_3Al_2Si_3O_{12}$ (M=Mg, Ca and Mn). Phys. Rev., B 64, 094302.

Mukhopadhyay, B., Holdaway, M.J., Koziol, A.M., 1997. A statistical model of thermodynamic mixing properties of Ca–Mg–Fe^{2+} garnets. Am. Mineral. 82, 165–181.

Nagel, T., de Capitani, C., Frey, M., 2002. Isograds and *P–T* evolution in the eastern Lepontine Alps (Graubünden, Switzerland). J. Metamorph. Geol. 20, 309–324.

Newton, R.C., Charlu, T.V., Kleppa, O.J., 1977. Thermochemistry of high-pressure garnets and clinopyroxenes in the system CaO–MgO–Al_2O_3–SiO_2. Geochim. Cosmochim. Acta 41, 369–377.

Purton, J.A., Barrera, G.D., Allan, N.L., Blundy, J.D., 1998. Monte Carlo and hybrid Monte Carlo/molecular dynamics approaches to order–disorder in alloys, oxides and silicates. J. Phys. Chem., B 102, 5202–5207.

Purton, J.A., Allan, N.L., Lavrentiev, M.Yu., Todorov, I.T., Freeman, C.L., 2005. Computer simulation of mineral solid solutions. Chem. Geol. 225, 176–188 doi:10.1016/j.chemgeo.2005.08.032.

Shannon, R.D., 1976. Revised effective ionic radii and systematic studies of interatomic distances in halides and chalcogenides. Acta Crystallogr., A 32, 751–767.

Sluiter, M.H.F., Vinograd, V., Kawazoe, Y., 2004. Intermixing tendencies in garnets: pyrope and grossular. Phys. Rev., B, 184120.

Taylor, M.B., Allan, N.L., Barron, T.H.K., Mackrodt, W.C., 1997. The free energy of formation of defects in polar solids. Faraday Discuss. 106, 377–387.

Taylor, M.B., Barrera, G.D., Allan, N.L., Barron, T.H.K., Mackrodt, W.C., 1998. SHELL—a code for lattice dynamics and structure optimisation of ionic crystals. Comput. Phys. Commun. 109, 135–143.

Thiéblot, L., Roux, J., Richet, P., 1998. High-temperature thermal expansion and decomposition of garnets. Eur. J. Mineral. 10, 7–15.

Todorov, I.T., Allan, N.L., Lavrentiev, M.Yu., Freeman, C.L., Mohn, C.E., Purton, J.A., 2004. Simulation of mineral solid solutions at zero and high pressure using lattice statics, lattice dynamics and Monte Carlo methods. J. Phys. Chem., B Condens. Mater. Surf. Interfaces Biophys. 16, S2751–S2770.

van Westrenen, W., Allan, N.L., Blundy, J.D., Purton, J.A., Wood, B.J., 2000. Atomistic simulation of trace element incorporation into garnets—comparison with experimental garnet–melt partitioning data. Geochim. Cosmochim. Acta 64, 1629–1639.

van Westrenen, W., Allan, N.L., Blundy, J.D., Lavrentiev, M.Yu., Lucas, B.R., Purton, J.A., 2003. Trace element incorporation into pyrope–grossular solid solutions: an atomistic simulation study. Phys. Chem. Miner. 30, 217–229.

Vinograd, V.L., Sluiter, M.H.F., Winkler, B., Putnis, A., Hálenius, U., Gale, J.D., Becker, U., 2004. Thermodynamics of mixing and ordering in pyrope–grossular solid solution. Min. Mag. 68, 101–121.

Walker, D., Cranswick, L.M.D., Verma, P.K., Clark, S.M., Buhre, S., 2002. Halite–sylvite thermoelasticity. Am. Mineral. 87, 805–812.

Wei, C., Powell, R., 2003. Phase relations in high-pressure metapelites in the system KFMASH (K_2O–FeO–MgO–Al_2O_3–SiO_2–H_2O) with application to natural rocks. Contrib. Mineral. Petrol. 145, 301–315.

Zhang, L., Ahsbahs, H., Kutoglu, A., 1998. Hydrostatic compression and crystal structure of pyrope up to 33GPa. Phys. Chem. Miner. 25, 301–307.

Zhang, L., Ahsbahs, H., Kutoglu, A., Geiger, C.A., 1999. Single-crystal hydrostatic compression of synthetic pyrope, almandine, spessartine, grossular and andradite garnets at high pressure. Phys. Chem. Miner. 27, 52–58.